



Full Text View

[Volume 29, Issue 4 \(April 1999\)](#)

Journal of Physical Oceanography

Article: pp. 807–820 | [Abstract](#) | [PDF \(212K\)](#)

Dense Water Formation beneath a Time-Dependent Coastal Polynya*

David C. Chapman

Woods Hole Oceanographic Institution, Woods Hole, Massachusetts

(Manuscript received March 6, 1998, in final form June 11, 1998)

DOI: 10.1175/1520-0485(1999)029<0807:DWFBAT>2.0.CO;2

ABSTRACT

Recent modeling studies of dense water formation beneath an idealized steady coastal polynya have provided simple analytical expressions for the maximum density anomaly achievable as a function of the polynya geometry and the imposed surface buoyancy flux. These studies have assumed that the buoyancy flux and polynya geometry are both constant and independent parameters. To relax these assumptions, dense water formation is examined beneath a coastal polynya whose size and surface buoyancy flux are computed from atmospheric temperature and wind velocity according to a polynya model developed by Pease. Though highly idealized, the Pease model produces polynyas that open and close on reasonably realistic timescales, and it thermodynamically couples the polynya size and buoyancy flux.

Results reveal several interesting and potentially useful features of the ocean response to time-dependent polynya forcing. First, under reasonable atmospheric conditions, both the maximum density anomaly achievable and the volume flux of dense water formed are nearly independent of polynya width and atmospheric temperature (and, therefore, surface buoyancy flux), but they are strongly dependent on the magnitude of the wind that pushes the ice offshore. Second, variations in polynya size produce horizontal gradients in surface buoyancy flux that are important in setting the scales of the ocean response. Third, timescales of the ocean response (>10 days) are typically longer than timescales associated with polynya openings and closings (a few days). Therefore, the ocean response to time-dependent polynya size and surface buoyancy flux is nearly the same as if the polynya size and surface buoyancy flux were fixed at the time average of the forcing (over 30–60 days). This suggests that reasonable estimates of dense water formed beneath Arctic polynyas may be possible by applying the simple expressions based on steady forcing, but using the seasonal averages of the parameters. Finally, it is difficult to find realistic combinations of atmospheric conditions that produce large quantities of water with density anomaly greater than about 1 kg m^{-3} .

Table of Contents:

- [Introduction](#)
- [Time-dependent ocean](#)
- [Time-dependent polynya](#)
- [Numerical results](#)
- [Discussion and summary](#)
- [REFERENCES](#)
- [APPENDIX](#)
- [TABLES](#)
- [FIGURES](#)

Options:

- [Create Reference](#)
- [Email this Article](#)
- [Add to MyArchive](#)
- [Search AMS Glossary](#)

Search CrossRef for:

- [Articles Citing This Article](#)

Search Google Scholar for:

- [David C. Chapman](#)

1. Introduction

It is generally accepted that dense water formed on Arctic continental shelves must play a leading role in the maintenance of the cold upper halocline in the deep Arctic basins, as first proposed by [Aagaard et al. \(1981\)](#), although the dynamics of the maintenance process largely remain a mystery. The required dense shelf water is believed to be produced primarily in regions of rapid and persistent ice growth, for example, coastal polynyas, in which brine rejection during ice formation acts as a negative buoyancy flux into the waters beneath. [Cavaliere and Martin \(1994\)](#) used available satellite, oceanographic, and atmospheric data to estimate that about 0.7–1.2 Sv ($\text{Sv} \equiv 10^6 \text{ m}^3 \text{ s}^{-1}$) of dense shelf water is produced within coastal polynyas over the entire Arctic; not enough to maintain the upper cold halocline, but a substantial fraction. Such estimates of dense shelf water production necessarily involve many assumptions because of the sparse data coverage in both space and time, as well as the difficulty of interpreting ice concentrations and growth rates. Another important source of uncertainty is that the ocean response is not considered in any detail. A given combination of surface buoyancy flux and polynya size is assumed to make a certain amount of dense water, but the ocean response to such complicated forcing is uncertain.

Several recent studies have begun to examine the ocean response beneath a steady coastal polynya and the subsequent offshore transport of dense water ([Gawarkiewicz and Chapman 1995](#); [Chapman and Gawarkiewicz 1995, 1997](#)). The approach has been to study the response in idealized settings in order to develop some basic understanding of the fundamental processes involved. Model results show that dense shelf water is carried rapidly offshore in a complicated field of small-scale (15–25 km) eddies, rather than a well-defined and organized plume. Despite the complex nature of the flow, scaling arguments based on the approach of [Visbeck et al. \(1996\)](#) have been used to derive simple algebraic expressions for the maximum density anomaly achievable beneath the polynya and the time required to reach this density anomaly, each in terms of the prescribed surface buoyancy flux and the polynya geometry. Even the unknown proportionality constant that was determined empirically in these studies has now been estimated theoretically ([Spall and Chapman 1998](#)), thereby providing a simple dynamically based estimate of the properties of dense water formed beneath a shallow coastal polynya.


These results are encouraging and potentially useful. However, the model polynyas of the previous studies have been highly simplified, so the general applicability of the results and simple expressions in more realistic situations is uncertain. The objective of the present work is to address three of the most obvious shortcomings of the previous studies:

- The surface buoyancy flux and the polynya geometry have been held fixed in both space and time. Natural polynyas open and close on timescales of a few days in response to varying winds and surface buoyancy fluxes, which are determined by changing atmospheric weather patterns and complicated ice dynamics. Model estimates of the time to reach the maximum density anomaly, based on the simple algebraic relationships with reasonably realistic parameter choices, are often considerably longer than the duration of typical polynya events, so it is unclear if the maximum density anomaly would ever be achieved.
- The surface buoyancy flux and the polynya geometry have been treated as independent parameters, clearly not the case in real polynyas. That is, large surface buoyancy fluxes tend to increase ice production that closes a polynya, while small surface buoyancy fluxes may allow a polynya to become exceptionally large. The two parameters should be thermodynamically coupled in model polynyas.
- The algebraic scaling relationships depend on the spatial structure of the surface buoyancy flux. In particular, the presence of a finite region over which the buoyancy flux decreases to zero away from the polynya (i.e., the so-called forcing decay region) changes the power law of the scaling ([Chapman and Gawarkiewicz 1997](#)), with the width of this region appearing as an important parameter in the scaling relationships (see [section 2](#) for more details). However, it is unclear exactly what the forcing decay region represents, how large it might be, and if it is a useful concept in more realistic situations.


To address these issues, the timescales of the ocean response to a steady polynya are examined first ([section 2](#)). Then, the idealized polynya model developed by [Pease \(1987\)](#) is used to introduce time dependence in the surface buoyancy flux and polynya size ([section 3](#)). More sophisticated and realistic polynya models have been constructed (e.g., [Ou 1988](#); [Markus and Burns 1995](#); [Lynch et al. 1997](#); [Willmott et al. 1997](#)), but the Pease model is adequate for this study. It is simple yet insightful, is easy to implement, produces polynyas that open and close on reasonably realistic timescales, and thermodynamically couples polynya size to surface buoyancy flux. Estimates of polynya size and surface buoyancy flux from the Pease model are then used as time-dependent forcing for a primitive-equation numerical model of the ocean response to a coastal polynya ([section 4](#)). The response to one case of “observed” forcing is also considered. Finally, results and implications are discussed and summarized ([section 5](#)).

2. Time-dependent ocean response to steady forcing

The timescales expected for the ocean response are revealed by considering a polynya with a constant surface buoyancy flux. Immediately upon applying the surface buoyancy flux, the density of the water directly beneath begins to increase. The density profile is then unstable, so the water mixes vertically. If the stratification is sufficiently weak that the dense water mixes to the bottom (i.e., the shallow convection case typical of Arctic coastal polynyas), then the increase in density is linear with time. A density front forms around the edge of the polynya and adjusts toward geostrophy, generating a rim current flowing around the edge of the polynya. The rim current is baroclinically unstable, so waves grow rapidly to finite amplitude, forming baroclinic eddies that propagate away from the rim current and exchange dense polynya water with lighter ambient water. If the forcing continues long enough, a quasi equilibrium is reached in which the buoyancy flux accompanying the eddy exchange balances the buoyancy loss at the surface, so the density beneath the polynya reaches an approximately constant value. If the surface buoyancy flux subsequently ceases, the eddies continue to exchange denser and lighter waters until the denser water is entirely mixed or carried away.

This well-known scenario may be expressed mathematically by following the approach that [Jones and Marshall \(1997\)](#) applied to deep convection [while keeping the notation of [Chapman and Gawarkiewicz \(1997\)](#)]. Consider a coastal polynya along a straight coastline ([Fig. 1](#) ) , occupying an area A over which a uniform surface buoyancy flux B_0 is imposed. The length of the polynya along the coast is $2a$, while the polynya extends offshore a distance b at its widest point. The buoyancy flux decreases to zero away from the polynya over a distance W , that is, the forcing decay region. The ocean has constant depth H and is initially unstratified with density ρ_0 . The total change in density beneath the polynya is determined by both the surface buoyancy flux and the lateral buoyancy flux associated with baroclinic eddies, and can be expressed as

$$\begin{aligned} \frac{d}{dt} \int \int \int \rho' dA dz \\ = \int \int \frac{\rho_0 B_0}{g} dA - \int \oint \overline{v' \rho'} dl dz, \end{aligned} \quad (1)$$

where ρ' is the density anomaly beneath the polynya, $\overline{v' \rho'}$ is the lateral eddy flux of density normal to the edge of the polynya, l is the distance along the edge of the polynya, z is the vertical coordinate, and g is gravitational acceleration. For simplicity, the buoyancy flux in the forcing decay region is ignored, so l refers to the edge of the constant flux region in [Fig. 1](#) .

The lateral density flux can be approximated as $\overline{v' \rho'} = c_e U \rho$, where U is the total geostrophic velocity along the rim current (i.e., the difference between the maximum surface and bottom velocities), $\rho = \int \int \int \rho' dA dz / AH$ is the spatially averaged density anomaly beneath the polynya, and c_e is an efficiency constant that can be viewed as the ratio of the speed of eddy propagation away from the rim current to the velocity of the rim current itself ([Spall and Chapman 1998](#)). The rim current velocity can be accurately estimated from the thermal wind ([Chapman 1998](#)), so $U = (gH/\rho_0 f)(\rho/W)$, where f is the Coriolis parameter which is assumed constant. Substituting these approximations into [\(1\)](#) and assuming that $\overline{v' \rho'}$ is independent of l and z yields

$$\frac{d\rho}{dt} + \left(c_e \frac{gH}{\rho_0 f W} \frac{P}{A} \right) \rho^2 = \frac{\rho_0 B_0}{gH}, \quad (2)$$

where P is the perimeter of the polynya along which eddy exchange occurs, that is, excluding the length at the coast.

The various possible balances in [\(2\)](#) demonstrate the expected ocean response to a steady coastal polynya. For example, immediately after the surface buoyancy flux is applied there are no eddies, so the eddy flux (second term on the left) is zero. Integrating [\(2\)](#) yields

$$\rho = \frac{\rho_0 B_0}{gH} t. \quad (3)$$

That is, the density beneath the polynya increases linearly with time. If the surface buoyancy flux is applied long enough, then a quasi-steady state is achieved in which the baroclinic eddy flux balances the surface flux and $d\rho/dt = 0$ in [\(2\)](#), producing the equilibrium density anomaly

$$\rho_e = \left(\frac{1}{c_e} \right) \frac{fW}{gH} \left(\frac{B_0}{P} \right)^{1/2}. \quad (4)$$

From (3), the time to reach the equilibrium density anomaly is

$$t_e = \left(\frac{1}{c_e} \right)^{1/2} \left(\frac{fWA}{B_0 P} \right)^{1/2}. \quad (5)$$

The estimates (4) and (5) are those obtained by [Chapman and Gawarkiewicz \(1997\)](#) but now generalized to an arbitrary polynya geometry. Note that [Visbeck et al. \(1996\)](#) obtained expressions analogous to (4) and (5) but for the case of $W = 0$, and these can be recovered by replacing W with the internal Rossby radius at equilibrium, $R_d = (\rho_e g H / \rho_0 f^2)^{1/2}$. The transition between the two cases has been investigated by [Chapman \(1998\)](#) and will not be considered here. Suffice it to say that W is here assumed large enough that (4) and (5) apply. If the surface buoyancy flux ceases at time t_c , then the right-hand side of (2) vanishes, leading to

$$\rho = \frac{\rho_c}{1 + \rho_c(t - t_c)/\rho_e t_e}, \quad (6)$$

where ρ_c is the density anomaly at time t_c . If $t_c > t_e$, then $\rho_c = \rho_e$, and (6) becomes

$$\rho = \frac{\rho_e}{1 + (t - t_c)/t_e}. \quad (7)$$

The ocean responds to polynya changes on the timescale t_e . At the onset of ice production (i.e., surface buoyancy flux), density increases linearly with time until equilibrium is approached at time t_e . After ice production ceases, eddies mix the dense water away with timescale $\rho_e t_e / \rho_c$, which is always greater than or equal to t_e . The scale t_e in (5) depends on the polynya geometry (through A and P) and the surface buoyancy flux. Examples of A and P for several idealized polynya shapes are shown in [Table 1](#). For typical parameter values [say, $B_0 = 2.5 \times 10^{-7} \text{ m}^2 \text{ s}^{-3}$, $b = 10 \text{ km}$, $W = 10 \text{ km}$, $f = 10^{-4} \text{ s}^{-1}$, and $c_e = 0.016$ based on [Chapman \(1998\)](#)], t_e ranges from 13 to 18 days depending on the particular geometry ([Table 1](#)). This is generally longer than the timescales associated with large polynya events (e.g., [Cavalieri and Martin 1994](#)), implying that the ocean probably cannot respond to rapid changes in polynya size and must, in some sense, integrate the polynya forcing. In general, $A/P \sim b$ and is nearly independent of the alongshore length of the polynya $2a$, consistent with [Chapman and Gawarkiewicz \(1997\)](#). This means that ρ_e in (4) depends on the product $B_0 b$, which is a measure of the total ice produced in a polynya and therefore the total salt rejected and available to increase the water density. The importance of this product will become clear later.

3. Time-dependent polynya

In the previous section, the polynya size and surface buoyancy flux were held constant and were treated as independent variables. To relax these constraints, the thermodynamical model of a latent heat coastal polynya developed by [Pease \(1987\)](#) is used to provide reasonably realistic polynya sizes and surface buoyancy fluxes that can then be used (in [section 4](#)) to force a numerical model of the ocean response.

a. The Pease model

Building on the ideas of [Lebedev \(1968\)](#), [Pease \(1987\)](#) considered the simplest conceptual scenario—the offshore width b of a polynya is determined by a competition between ice formation tending to close the polynya and wind tending to open the polynya by blowing the ice offshore. The alongshore extent of the polynya is assumed infinite, corresponding to the “infinite strip” polynya in [Table 1](#). The Pease model can be written in terms of the surface buoyancy flux as

$$\frac{db}{dt} + \frac{B_0}{\kappa} b = V_i = 0.03 V_a, \quad (8)$$

where V_i is the offshore speed of the ice, taken to be 3% of the offshore wind speed V_a , and $\kappa = \Delta \rho_s g h / \rho_0$ where $\Delta \rho_s$ is

the density change resulting from salt rejection, and h_i is the so-called collection depth of the newly formed frazil ice. There is considerable uncertainty in estimates of h_i , but a value of about 0.1 m appears to be reasonable (Markus and Burns 1995) and is used here. The density change for $\rho_0 = 1025 \text{ kg m}^{-3}$, assuming 69% of the salt is rejected, is $\Delta\rho_s = 17.25 \text{ kg m}^{-3}$, leading to $\kappa = 0.0165 \text{ m}^2 \text{ s}^{-2}$. For the present purposes, κ is considered constant at this value.

The surface buoyancy flux is determined by the ice production rate and can be written:

$$B_0 = -\frac{\Delta\rho_s}{\rho_0 g} \frac{Q}{\rho_i L_f}, \quad (9)$$

where Q is the total surface heat flux from the atmosphere to the ocean, $\rho_i = 0.95 \times 10^3 \text{ kg m}^{-3}$ is the density of young sea ice, and $L_f = 3.34 \times 10^5 \text{ J kg}^{-1}$ is the latent heat of freezing for salt water. The surface heat flux is given by

$$Q = Q_{ld} - Q_{lu} + Q_s + Q_e - Q_r, \quad (10)$$

where Q_{ld} , Q_{lu} are the downward and upward longwave radiation, respectively, Q_s is the sensible or turbulent heat flux, Q_e is the evaporative heat flux, and Q_r is the solar radiation. Following Pease (1987), Q_{lu} is assumed constant and equal to 301 W m^{-2} because the surface water is always nearly freezing at $T_w = -1.8^\circ\text{C}$; Q_r is neglected because it is nearly zero at high latitudes during winter; Q_e is ignored because it is smaller than the uncertainty in Q_s ; $Q_{ld} = \sigma e_a (273^\circ\text{C} + T_a)^4$, where $\sigma = 5.67 \times 10^{-8} \text{ W m}^{-2} \text{ }^\circ\text{C}^{-4}$ is the Stefan–Boltzmann constant, $e_a = 0.95$ is an effective emmissivity for the air, and T_a is the air temperature in $^\circ\text{C}$; and $Q_s = \rho_a C_h C_p |V_a| (T_a - T_w)$, where $\rho_a = 1.3 \text{ kg m}^{-3}$ is the air density, $C_h = 0.002$ is a sensible heat coefficient, $C_p = 1004 \text{ J }^\circ\text{C}^{-1} \text{ kg}^{-1}$ is the specific heat of air, and $|V_a|$ is the magnitude of the wind velocity. Substitution into (9) and (10) yields

$$B_0 = -[\sigma e_a (273^\circ\text{C} + T_a)^4 - Q_{lu} + \rho_a C_h C_p |V_a| (T_a - T_w)] \times \Delta\rho_s / \rho_0 g \rho_i L_f. \quad (11)$$

From (11), the surface buoyancy flux depends on both the air temperature and the wind speed, so T_a and V_a have become the variables that force the polynya model (8).

b. Constant forcing

The solution of (8) with constant T_a and V_a (and, therefore, constant B_0) is

$$b = \frac{0.03\kappa V_a}{B_0} (1 - e^{-tB_0/\kappa}). \quad (12)$$

The polynya opens from $b = 0$ to the maximum width

$$b_{\max} = 0.03\kappa V_a / B_0 \quad (13)$$

with timescale κ/B_0 . Pease (1987) investigated this case extensively. For reasonable values of T_a and V_a , the opening timescale is less than one day, so the polynya nearly reaches b_{\max} within 1–2 days. For example, for $T_a = -20^\circ\text{C}$ and $V_a = 10 \text{ m s}^{-1}$, (11) produces $B_0 = 2.9 \times 10^{-7} \text{ m}^2 \text{ s}^{-3}$ from which the opening timescale is $\kappa/B_0 = 0.66$ days and the maximum polynya width is $b_{\max} = 17.1 \text{ km}$. The polynya opens quickly relative to the ocean response timescale of more than 10 days, indicating that forcing a model with a suddenly imposed surface buoyancy flux over the entire polynya width, as done in previous studies, is a reasonable approximation.

During the opening process, the length of time that the ocean is exposed to the surface buoyancy flux decreases with

distance offshore. That is, the region near the coast is exposed for the entire opening time, while the seaward edge of the polynya is always just being exposed as the polynya expands. This creates an offshore density gradient that in turn produces an alongshore geostrophic current. However, the polynya opens so rapidly that the density gradient and current are both small and can be ignored in the ocean response (see the appendix).

[Figure 2](#) shows the surface buoyancy flux B_0 from (11) and the maximum polynya width b_{\max} from (13) computed over a wide range of air temperatures and wind speeds. The buoyancy flux varies by nearly an order of magnitude with the largest fluxes occurring for the coldest air temperatures and the strongest winds. The maximum polynya width, on the other hand, is nearly independent of wind speed and only moderately dependent on air temperature, except at the warmest temperatures. Typical values of b_{\max} range from 10 to 30 km. The weak dependence of b_{\max} on V_a reflects the competing roles of the wind in opening the polynya; it pushes the ice offshore, which opens the polynya, but it also contributes to the surface buoyancy flux, which tends to close the polynya.

The steady or maximum polynya width, given by (13), can be used to estimate the ocean equilibrium response (4) and (5). As mentioned above, the maximum density anomaly achievable, given by (4), depends on the product $B_0 b$, which from (13) is $0.03\kappa V_a$. Thus, ρ_e depends on the offshore wind speed but is independent of the air temperature! That is, the rate at which ice moves offshore determines how dense the water can become, not the air temperature or the polynya width, implying that the presence of a very large polynya or very cold air temperature does not necessarily mean that unusually dense water is being formed. The reason is that cold air temperatures lead to rapid ice production, which both increases brine rejection and reduces the polynya size; two responses that have opposite impacts on dense water formation, essentially canceling their effects. [This result has been independently recognized by [van Woert \(1998\)](#).] According to (5) with (13), the time required to reach the maximum density anomaly t_e is inversely proportional to B_0 , so ρ_e is more likely to be achieved when the air temperature is cold.

c. Time-dependent forcing

The polynya response to time-dependent air temperature and wind speed and its impact on dense water formation, through the product $B_0 b$, are examined here. A general analytical solution for (8) with arbitrary air temperature and wind speed is

$$b = \exp\left(-\int B_0/\kappa dt\right) \left[\int V_i \exp\left(\int B_0/\kappa dt'\right) dt + C \right], \quad (14)$$

where C is a constant of integration determined from the initial conditions. However, the complicated relationship among T_a , V_a , and B_0 makes (14) difficult to evaluate except for the simplest cases, so solutions of (8) presented here have been obtained numerically using a one-step Runge–Kutta scheme available in MATLAB.

For simplicity, T_a and V_a are treated as independent variables. The air temperature is assumed periodic with a mean offset

$$T_a = T_0 + T_1 \cos(\omega_T t), \quad (15)$$

where T_0 is the mean air temperature, T_1 is the amplitude of the oscillation, and ω_T is the frequency of oscillation. The wind is more complex because it appears in (8) and (11) as both the offshore wind speed and the magnitude of the wind speed. The offshore wind speed varies due to changes in wind direction as well as changes in magnitude. To represent this in a simple way, the wind is assumed to have the form

$$\begin{aligned} V_a &= |V_a| \cos(\omega_o t) \\ &= [V_0 + V_1 \cos(\omega_m t)] \cos(\omega_o t), \end{aligned} \quad (16)$$

where V_0 and V_1 are constants, ω_m is the frequency of wind magnitude variations, and ω_o is the frequency of offshore wind oscillations. This choice corresponds to a wind that rotates direction with frequency ω_o while changing magnitude with amplitude V_1 and frequency ω_m about a mean of V_0 . If V_a becomes negative, that is, onshore, then V_a is set to zero

for the integration of (8). These forms for T_a and V_a are clearly artificial, but they lead to interesting and not unrealistic responses.

There are, of course, unlimited choices for air temperature and wind speed using (15) and (16). After examining many solutions of (8) for such choices, the polynya responses can be grouped into two broad categories: 1) *persistent polynyas* that open rapidly and remain open while continually changing size and 2) *intermittent polynyas* that repeatedly open and completely close during the forcing period. These two categories are roughly consistent with the types of observed Arctic polynyas suggested by [Stringer and Groves \(1991\)](#) based on Advanced Very High Resolution Radiometer imagery. The difference between the polynya responses is determined by whether or not the offshore wind speed reverses; an onshore wind allows ice formation to completely close the polynya.

[Figure 3](#) shows the response typical of a persistent polynya over 40 days of forcing. In this case, the frequency of the offshore wind speed oscillation was set to zero, that is, $\omega_o = 0$ in (16), so $V_a = |V_a|$ and oscillates between 0 and 24 m s^{-1} with a period of 4 days ([Fig. 3a](#)). The air temperature oscillates between -28.2° and -1.8°C with a period of 5 days ([Fig. 3b](#)). Thus, the wind speed V_a and surface buoyancy flux B_0 each oscillate between zero and a maximum, but with different periods so that different combinations of the two occur through the forcing period, repeating the pattern every 20 days. The resulting surface buoyancy flux ([Fig. 3c](#)) varies from 0 to about $9 \times 10^{-7} \text{ m}^2 \text{ s}^{-3}$. As expected, it tends to be largest when the wind is strong and the air is cold. It vanishes when the air and water temperatures are identical and is small when the wind vanishes. The polynya width ([Fig. 3d](#)) is irregular, changing from a minimum of about 12 km to a maximum of about 80 km. As expected from the steady solutions, there is a tendency for B_0 and b to vary inversely, at least on an event-by-event basis. That is, the width is small (large) when the surface buoyancy flux is large (small). The largest polynyas occur when B_0 is small and V_a is nonzero (e.g., days 11 and 31); then the ice can be pushed far offshore before new ice production can close the polynya. Conversely, the polynya is rapidly reduced to its minimum size when the wind is weak and the buoyancy flux is strong (e.g., days 3 and 18).

[Figure 3e](#) shows the product $B_0 b$ as a measure of both total ice production and the maximum density anomaly achievable. The large variability indicates that B_0 and b are not as simply related as suggested by (13). Total ice production obviously vanishes when B_0 vanishes. Ice production is largest either when B_0 is large and b is small (e.g., days 2 and 18) or when B_0 and b are each in their midrange of values (e.g., days 7 or 14). Ice production can be small even when the polynya is wide (e.g., days 10 and 30).

[Figure 4](#) shows the response typical of an intermittent polynya over 40 days of forcing. Here, the offshore wind speed oscillates with a period of 5 days ([Fig. 4a](#)), while the wind magnitude oscillates between 10 and 22 m s^{-1} with a period of 6 days ([Fig. 4b](#)). This ensures that the wind magnitude never vanishes, but the offshore wind reverses direction. The air temperature oscillates between -35° and -15°C with a period of 7.5 days ([Fig. 4b](#)). The surface buoyancy flux ([Fig. 4c](#)) varies between 0 and about $10^{-6} \text{ m}^2 \text{ s}^{-3}$, again with largest values when $|V_a|$ is large and the air is cold (e.g., days 3, 27, and 33). The polynya width ([Fig. 4d](#)) is more regular than in the persistent polynya case and varies within a smaller range, from 0 to about 20 km. The regularity results from the rapid response of the polynya to changes in the forcing; that is, the polynya closely follows the forcing. Therefore, the polynya closes completely when the offshore wind vanishes for a few days, and it opens when the wind turns offshore again. Interestingly, the two largest polynya widths occur under different circumstances. On day 15, the surface buoyancy flux is of medium size, but the offshore wind is at maximum strength, driving the ice well offshore. On day 30, the wind is about half the strength of day 15, but the surface buoyancy flux nearly vanishes, so the moderate wind can still open the polynya nearly as wide as on day 15. The amount of ice produced in these two periods is also different; [Fig. 4e](#) shows that $B_0 b$ on day 15 is about twice that on day 30.

Similarly, periods of nearly identical polynya variations may vary by a factor of 2 in ice production (e.g., days 4–7 compared with days 9–12). Therefore, simply observing the polynya width does not indicate how much ice is being produced. [Figure 4e](#) also shows the dominance of offshore wind speed in determining ice production, as suggested by (13); times of largest ice production all correspond to times of strongest offshore winds.

4. Numerical results

The ocean response to rapid variations of the thermodynamically coupled surface buoyancy flux and polynya width is examined here by forcing a primitive-equation numerical ocean model with the solutions found in [section 3](#). The calculations follow closely the approach of [Chapman and Gawarkiewicz \(1997\)](#).

a. Model description

The numerical model is the semispectral primitive equation model described by [Haidvogel et al. \(1991\)](#). The model domain is a high-latitude, uniformly rotating ($f = 1.3 \times 10^{-4} \text{ s}^{-1}$), straight channel with periodic boundaries at the open ends. The domain is $100 \text{ km} \times 100 \text{ km}$ with 1-km resolution in each direction. The ocean has uniform depth, $H = 50 \text{ m}$, and nine Chebyshev polynomials are used to resolve the vertical structure. Standard dynamical assumptions are made: rigid lid, no flow or density flux through solid boundaries, no stress at the solid boundaries or the surface, a Richardson-number-based vertical mixing coefficient, convective adjustment to mix the density field whenever it is statically unstable, and small lateral Laplacian subgrid-scale mixing to ensure numerical stability. Further model details may be found in [Chapman and Gawarkiewicz \(1997\)](#).

Each calculation begins from rest with a homogeneous ocean with density ρ_0 . At time $t = 0$, a surface buoyancy flux B_0 is applied in a strip along the entire channel, adjacent to the coast and extending a distance b offshore. The values of B_0 and b vary in time according to the solutions obtained from the Pease model ([section 3](#)). The surface buoyancy flux decreases sharply to zero within 1 km offshore of b . That is, there is essentially no explicitly imposed forcing decay region at each instant in time. Thus, if B_0 and b were to remain constant in time, the scales for shallow, internally constrained convection ([Chapman 1998](#)) would apply instead of [\(4\)](#) and [\(5\)](#). Each calculation is halted before eddies reach the offshore boundary.

b. Response to a persistent polynya

The ocean response to a persistent polynya is examined first by forcing the numerical model with the Pease model solution shown in [Fig. 3](#). [Figure 5](#) shows the density anomaly at the bottom at selected times during the 40-day calculation. Despite the large variations in B_0 and b , the development is remarkably similar to that with steady forcing. Near the coast, where the polynya remains open at 10–15 km, the density increases steadily. By day 10, small eddies have formed along the edge of this persistently open region. Larger eddies develop by day 20, after which the domain continues to fill with eddies.

In this case, the polynya width varies considerably, twice nearly crossing the entire model domain ([Fig. 3d](#)). The primary effect of the varying polynya width is to create a wide region of decreasing density anomaly, much like that found beneath a forcing decay region, despite the absence of such a region here. This is illustrated in [Fig. 6](#), where the surface buoyancy flux, averaged over the 40-day period, is plotted as a function of distance offshore. The persistently open region extends 12.5 km from the coast and has a nearly uniform average buoyancy flux of $B_0 \approx 2.5 \times 10^{-7} \text{ m}^2 \text{ s}^{-3}$. Offshore of this uniform region, the average surface buoyancy flux decreases almost exponentially with an e -folding scale of about 7.5 km (dashed curve), appearing like a forcing decay region.

The ocean response is represented by the time history of the density anomaly near the coast averaged along the channel and within 4 km of the coast (solid curve in [Fig. 7](#)). For about 23 days, the density anomaly simply increases in response to the surface buoyancy flux. The response for the first 20 days is nearly identical to the time integral of [\(2\)](#) using the imposed surface buoyancy flux and neglecting the eddy flux term (not shown). By day 25, the baroclinic eddies ([Fig. 5](#)) have become dominant, and equilibrium is reached with a quasi-steady density anomaly of $\rho_e \approx 0.9 \text{ kg m}^{-3}$.

An identical calculation was made in which the forcing was held steady at approximately the 40-day average shown in [Fig. 6](#); that is, $B_0 = 2.5 \times 10^{-7} \text{ m}^2 \text{ s}^{-3}$ within 12.5 km of the coast, beyond which B_0 decays exponentially with an e -folding scale of 7.5 km (dashed curve in [Fig. 6](#)). The resulting density anomaly near the coast (dashed curve in [Fig. 7](#)) roughly follows the response to the time-dependent forcing, confirming that the slow ocean response integrates the higher frequency forcing of the polynya events. Furthermore, the average forcing values can be used to estimate the equilibrium density anomaly and timescale according to [\(4\)](#) and [\(5\)](#) (infinite strip in [Table 1](#) with $B_0 = 2.5 \times 10^{-7} \text{ m}^2 \text{ s}^{-3}$, $b = 12.5 \text{ km}$, $W = 7.5 \text{ km}$, $\rho_0 = 1000 \text{ kg m}^{-3}$, and $c_e = 0.016$),¹ producing $\rho_e = 0.9 \text{ kg m}^{-3}$ and $t_e = 20 \text{ days}$, both of which are in good agreement with [Fig. 7](#). This suggests that the steady results could be used to estimate the properties of dense water formed beneath a time-dependent persistent polynya by using the seasonally averaged values of the surface buoyancy flux and its offshore distribution.

A third calculation was made in which the forcing was steady, but the forcing decay region was absent; that is, $B_0 = 2.5 \times 10^{-7} \text{ m}^2 \text{ s}^{-3}$ within 12.5 km of the coast and zero farther offshore. The resulting density anomaly near the coast (dotted curve in [Fig. 7](#)) shows that equilibrium is reached after about 15 days with an equilibrium density anomaly of about 0.6 kg m^{-3} , considerably less than that obtained with the forcing decay region. These are close to the theoretical values of $\rho_e = 0.69 \text{ kg m}^{-3}$ and $t_e = 15.6 \text{ days}$, obtained by substituting $R_d = (\rho_e g H / \rho_0 f^2)^{1/2}$ for W in [\(4\)](#) and [\(5\)](#). Thus, the time-varying

polynya width produces an effective forcing decay region that sets the horizontal scale of the rim current, thereby slowing eddy development and allowing a larger increase in density beneath the polynya, in agreement with [Chapman and Gawarkiewicz \(1997\)](#) and [Chapman \(1998\)](#).

c. Response to an intermittent polynya

The ocean response to an intermittent polynya is examined by forcing the numerical model with the Pease model solution shown in [Fig. 4](#). The density anomaly at the bottom is shown in [Fig. 8](#) at several times during the 40-day calculation. The overall behavior is qualitatively similar to the persistent polynya ([Fig. 5](#)), except that there is no region of constant forcing near the coast because the polynya completely closes about every 5 days. That is, the entire area beneath the polynya has strong cross-shelf density gradients and resembles a forcing decay region adjacent to the coast. As a result, the baroclinic eddies modify the density at the coast as soon as they form, so equilibrium is expected to be reached more rapidly.

The 40-day average surface buoyancy flux as a function of distance offshore is shown in [Fig. 9](#); it decreases rapidly over the first kilometer and then almost linearly before nearly vanishing at about 12–13 km offshore. This structure precludes the application of (4) and (5) because they were derived after neglecting the buoyancy flux in the forcing decay region relative to that in the constant flux region (see [Chapman and Gawarkiewicz 1997](#); [Chapman 1998](#)). Here, all the buoyancy flux occurs in the forcing decay region. Furthermore, the theoretical estimate of c_e from [Spall and Chapman \(1998\)](#) may not apply. Therefore, no attempt is made here to predict the equilibrium values ρ_e and t_e for the intermittent polynya.

[Figure 10](#) shows the density anomaly near the coast in response to the intermittent polynya (solid curve) and the response to a steady surface buoyancy flux (dashed curve) that approximates the time average of the variable forcing [$B_0 = 3.5 \times 10^{-7} \text{ m}^2 \text{ s}^{-3}$ at the coast and decreasing linearly to zero at 13 km offshore (dashed curve in [Fig. 9](#))]. The responses differ in detail, as expected, but they are fairly close in terms of the time at which equilibrium is approached as well as the quasi-steady equilibrium density anomaly. Again, this supports the contention that the ocean responds to the average polynya forcing rather than the rapid variations in polynya width and surface buoyancy flux. These calculations also clearly support the importance of the forcing decay region because without it there would be no surface buoyancy flux.

d. Spindown

If the surface buoyancy flux ceases, exchange by baroclinic eddies continues until the dense water is completely carried away or mixed with ambient water. The decay of the density anomaly should, in principle, follow (6) or (7), depending on when the surface buoyancy flux ceases. To test this idea, both the persistent and intermittent polynya calculations described above were repeated, but now setting the surface buoyancy flux to zero at some time after the equilibrium has been reached. [Equation \(7\)](#) should apply in both cases.




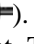
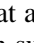
The responses are shown by solid curves in [Fig. 11](#). The dashed curves show the decay according to (7); $\rho_e = 0.9 \text{ kg m}^{-3}$, $t_e = 20 \text{ days}$, $t_c = 30 \text{ days}$ for the persistent polynya ([Fig. 11a](#)) and $\rho_e = 0.6 \text{ kg m}^{-3}$, $t_e = 13 \text{ days}$, $t_c = 26.5 \text{ days}$ for the intermittent polynya ([Fig. 11b](#)). (In [Fig. 11a](#) the decay curve has been shifted slightly upward so as to start at the actual density anomaly at day 30.) In both cases, the spindown of the polynya system is close to the theoretical prediction, supporting the validity of the eddy exchange model of [section 2](#).

e. Response to “observed” forcing

Observed polynya widths and surface buoyancy fluxes that would be needed to impose realistic forcing on the numerical model are not readily available. Nevertheless, proxies for these quantities can be estimated from observed air temperatures and winds near a polynya, combined with polynya sizes derived from satellite observations. An example of such data is described by [Weingartner et al. \(1998\)](#) for the northeast Chukchi Shelf during the winter of 1991/92. The surface heat flux is computed using (10) in essentially the same way as described in [section 3](#). A buoyancy flux is then estimated according to (11). The polynya width is approximated from the open water area computed by [Weingartner et al](#) by assuming that the polynya extends a uniform distance from the coast over the entire 350-km length of coastline considered in the satellite imagery; that is, polynya width equals open water area divided by 350 km. Further details of the data gathering and processing are explained by [Weingartner et al](#)

The “observed” daily mean forcing variables are shown in [Fig. 12](#) for a 60-day subset of the [Weingartner et al](#) dataset, beginning on 20 December 1991. The “observed” polynya is like an intermittent polynya in that the offshore wind reverses occasionally ([Fig. 12a](#)) and the polynya width nearly vanishes several times ([Fig. 12d](#)). The “observed” polynya


width never actually vanishes because it is estimated from the total open water in the region, whether or not it is adjacent to the coast. So, it is almost certainly an overestimate of the true opening. The largest ice production $B_0 b$ occurs when the polynya is widest because both the offshore wind and the surface buoyancy flux are substantial.

The average buoyancy flux (Fig. 13 ) looks like a cross between the persistent and intermittent polynyas. There is a narrow region near the coast (1.5 km) where the buoyancy flux is nearly constant at $B_0 \approx 2.7 \times 10^{-7} \text{ m}^2 \text{ s}^{-3}$, adjoining a region of nearly exponential offshore decay with an e -folding scale of about 12 km. Figure 14  shows the ocean response to the “observed” surface buoyancy flux and polynya width (linearly interpolating the curves in Fig. 12  to get values at each time step) and the response to an approximate 60-day average forcing (dashed curve in Fig. 13 ). As in the previous examples, the equilibrium density anomalies are similar, although the transition to equilibrium is different. The time-dependent forcing takes longer to reach equilibrium because the largest contributions to the average come from the two events centered on days 20 and 30 (Fig. 12 ) that are, by definition, included in the average forcing from the beginning of the calculation. Thus, this more realistic case again supports the idea that the ocean basically responds to the average polynya forcing.

5. Discussion and summary

The objective of this work was to address three shortcomings of previous studies of dense water formation beneath coastal polynyas; namely, (i) steady forcing, (ii) independence of surface buoyancy flux and polynya width, and (iii) lack of evidence and/or meaning for the forcing decay region. To address these shortcomings, a few calculations have been presented that are representative of a larger number of similar calculations that have been made using a wide range of parameters. Taken together, the results shed light on all three of the issues.

First, the typical ocean response timescale is determined by the dynamics of baroclinic eddies and their efficiency in exchanging dense water from beneath the polynya with ambient water. A typical ocean adjustment timescale is greater than 10 days; longer than typical polynya event timescales, which are determined primarily by regional weather patterns. Therefore, the ocean tends to integrate the polynya forcing over many events, as shown by the numerical calculations that use steady forcing equal to the average of the time-dependent forcing and yield similar results, especially in terms of the maximum density anomaly achieved. This suggests that the simple scaling relationships (4) and (5), based on steady forcing, could be used to estimate dense water formation beneath persistent coastal polynyas over a longer time period (e.g., an entire winter) by using the average parameter values. This approach has been taken by [Martin et al. \(1998\)](#) in an investigation of dense water formation beneath polynyas in the Okhotsk Sea with encouraging results. For intermittent coastal polynyas, new theoretical estimates of the equilibrium water properties [like (4) and (5)] are needed, and then the same approach may be applicable, provided that the time between polynya events is shorter than t_e . Otherwise, the ocean will have time to respond between events and the averaging approach may be invalid.

Second, the Pease model of a latent heat coastal polynya shows that the surface buoyancy flux and polynya width are tightly coupled, providing strong constraints on the parameters as they appear in the equilibrium relationships (4) and (5). In particular, for constant forcing the equilibrium density predicted by (4) is independent of both air temperature and polynya width because $B_0 b$ depends only on the offshore wind speed according to (13). This means that large polynyas and/or cold air temperatures alone do not indicate the formation of large amounts of dense water. Instead, persistent polynyas with strong offshore winds and cold air temperatures tend to produce the greatest increase in water density. These polynyas tend to be relatively small, $b \approx 10\text{--}20$ km from Fig. 2 , which implies the need for improved small-scale resolution in estimates of ice cover based on remote sensing approaches. Many satellite instrument footprints are as large or larger than the offshore scale of these polynyas, suggesting that past estimates of open water area may have missed some of the most important sites of dense water formation.

Third, the present results support the contention that the forcing decay region is important in setting the scales of the ocean response, as suggested by [Chapman and Gawarkiewicz \(1997\)](#). Here, no explicit forcing decay region was imposed, but time variations in polynya width exposed the water to the surface buoyancy flux for different lengths of time, producing cross-shelf density gradients over a substantial region and thereby an effective forcing decay region that is important in determining ρ_e and t_e . Thus, the forcing decay region used with steady forcing may be interpreted as the region over which the polynya width changes in time. Alternatively, a forcing decay region may form as a consequence of spatial variations in large-scale forcing or ice dynamics. Such a region could be included explicitly in calculations like those in [section 4](#), and it would probably widen the effective forcing decay region and increase ρ_e . In any case, the presence of a forcing decay region is likely to be important in natural polynyas. For example, [Martin et al. \(1998\)](#) used the concept of the forcing decay region to represent the large areas of thin ice typically surrounding Okhotsk Sea polynyas and found it to be an important contributor to the estimates of dense water formation.

The present results can be used to estimate the volume rate of dense water production from a coastal polynya. With steady forcing (e.g., this could be the seasonal average), the density in the volume of water beneath the polynya is increased

by an amount ρ_e in time t_e . Afterward, the eddies carry water away, and the polynya must continue to produce water with the equilibrium density anomaly at the same rate to maintain the equilibrium. So, the volume flux F of dense water at equilibrium is given by the polynya volume divided by t_e , or

$$F = AH/t_e = c_e^{1/2} H \left(\frac{B_0}{fW} AP \right)^{1/2}, \quad (17)$$

where (5) has been used. From Table 1, $AP \sim ba^2$ indicating that the volume flux increases linearly with both the water depth and the alongshore length of the polynya. That is, longer polynyas over deeper shelves tend to make more dense water. However, ρ_e is proportional to H^{-1} , so the density anomaly will be reduced on deeper shelves. Conversely, very dense water can be made in shallow regions, but the volume flux will be greatly reduced. The linear dependence of AP on b means that the product $B_0 b$ appears again in (17), so the volume flux of dense water tends to be independent of air temperature and polynya width, as is ρ_e . A typical value of F based on the calculations presented here is $F \approx 0.04$ Sv per 100 km of coastal polynya. So, the equivalent of about 25 such lengths of polynya would be needed to produce 1 Sv of dense water, possibly available for maintaining the cold upper halocline if the water has the proper density.

The equilibrium density anomalies achieved in the model calculations presented here are all about 1 kg m^{-3} or less. This is also true for the numerous similar calculations that have been made, suggesting (speculatively) that reasonably realistic polynyas may not produce enough ice for extended periods of time to increase the density by more than about 1 kg m^{-3} . The density anomaly could, of course, be increased by decreasing the ocean depth, but this would decrease the volume flux of dense water formed [according to (17)], so such a shallow polynya would probably not be an important source of dense water. Thus, only in extreme conditions can a coastal polynya make water dense enough to sink to the bottom of the deep Arctic basins, which may account for the small amounts of Arctic bottom water that appear to originate over the shelves. This also lends support to the idea that the dense shelf water can maintain the cold upper halocline, because the density increase is about the right size. Of course, the calculations presented here provide estimates of the density anomaly, so the ambient density at the beginning of winter is of paramount importance to the maximum density produced during the winter.

From an observational standpoint, the present results suggest that estimates of dense water formation require measurements of polynya size, air temperature, wind velocity, and ambient water density. It appears that gross estimates of seasonal dense water formation do not require detailed oceanographic surveys of dense water fluxes away from the polynyas. This is encouraging for prospects of long-term monitoring and observations of global change. Furthermore, the ideas presented here could be tested relatively simply by measuring polynya size from satellites, air temperature, and wind velocity at the coast and ocean water properties from a single moored CTD near the coast. Is an equilibrium density anomaly achieved? If so, is it close to that estimated from (4)? Of course, other aspects of the modeling results should be tested, for example, eddy sizes and structures, frontal scales, and velocities, etc., which would probably require a large-scale field program. If successful, simple relationships like (4) and (5) could be used for examining interannual variability in dense water formation using historical data, for predicting global change scenarios, and perhaps for incorporating shelf processes into basin-scale numerical models that are presently incapable of resolving coastal polynyas and their effects.

Finally, it is important to remember that many simplifications have been made in the present study. Bottom topography, stratification, bottom friction, wind forcing of ocean currents, ambient ocean currents, and ice dynamics have all been ignored. Bottom topography and bottom friction are known to alter the estimates of ρ_e and t_e by changing c_e (Chapman and Gawarkiewicz 1997; Chapman 1998). Wind forcing and ambient ocean currents may also have an important impact on the results and should certainly be considered in future studies.

Acknowledgments

I thank Tom Weingartner, Glen Gawarkiewicz, and Steve Lentz for numerous fruitful discussions and helpful comments concerning this work. I additionally thank Tom Weingartner for generously sharing the Chukchi Shelf data. Financial support was provided by the National Science Foundation (NSF) as part of the Arctic System Science (ARCSS) program which is administered through the Office of Polar Programs (Grant OPP-9422292).

REFERENCES

Cavaleri, D. J., and S. Martin, 1994: The contributions of Alaskan, Siberian, and Canadian coastal polynyas to the cold halocline layer of the Arctic Ocean. *J. Geophys. Res.*, **99**, 18 343–18 362..

Chapman, D. C., 1998: Setting the scales of the ocean response to isolated convection. *J. Phys. Oceanogr.*, **28**, 606–620.. [Find this article online](#)

—, and G. Gawarkiewicz, 1995: Offshore transport of dense shelf water in the presence of a submarine canyon. *J. Geophys. Res.*, **100**, 13 373–13 387..

—, and —, 1997: Shallow convection and buoyancy equilibration in an idealized coastal polynya. *J. Phys. Oceanogr.*, **27**, 555–566.. [Find this article online](#)

Gawarkiewicz, G., and D. C. Chapman, 1995: A numerical study of dense water formation and transport on a shallow, sloping continental shelf. *J. Geophys. Res.*, **100**, 4489–4507..

Haidvogel, D., J. Wilkin, and R. Young, 1991: A semi-spectral primitive equation ocean circulation model using vertical sigma and orthogonal curvilinear horizontal coordinates. *J. Comput. Phys.*, **94**, 151–185..

Jones, H., and J. Marshall, 1997: Restratification after deep convection. *J. Phys. Oceanogr.*, **27**, 2276–2287.. [Find this article online](#)

Lebedev, V. L., 1968: Maximum size of a wind-generated lead during sea freezing. *Oceanology* (Engl. Transl.), **8**, 313–318..

Lynch, A. H., M. F. Glueck, W. L. Chapman, D. A. Bailey, and J. E. Walsh, 1997: Satellite observation and climate system model simulation of the St. Lawrence Island polynya. *Tellus*, **49A**, 277–297..

Markus, T., and B. A. Burns, 1995: A method to estimate subpixel-scale coastal polynyas with satellite passive microwave data. *J. Geophys. Res.*, **100**, 4473–4487..

Martin, S., R. Drucker, and K. Yamashita, 1998: The production of ice and dense shelf water in the Okhotsk Sea polynyas. *J. Geophys. Res.*, **103**, 27 771–27 782..

Ou, H. W., 1988: A time-dependent model of a coastal polynya. *J. Phys. Oceanogr.*, **18**, 584–590.. [Find this article online](#)

Pease, C. H., 1987: The size of wind-driven coastal polynyas. *J. Geophys. Res.*, **92**, 7049–7059..

Spall, M. A., and D. C. Chapman, 1998: On the efficiency of baroclinic eddy heat transport across narrow fronts. *J. Phys. Oceanogr.*, **28**, 2275–2287.. [Find this article online](#)

Stringer, W. J., and J. E. Groves, 1991: Location and areal extent of polynyas in the Bering and Chukchi Seas. *Arctic*, **44**, 164–171..

van Woert, M. L., 1998: The wintertime expansion and contraction of the Terra Nova Bay polynya. *Oceanography of the Ross Sea-Antarctica*, G. M. R. Manzella and G. Spezie, Eds., Springer-Verlag, in press..

Visbeck, M., J. Marshall, and H. Jones, 1996: Dynamics of isolated convective regions in the ocean. *J. Phys. Oceanogr.*, **26**, 1721–1734.. [Find this article online](#)

Weingartner, T. J., D. J. Cavalieri, K. Aagaard, and Y. Sasaki, 1998: Circulation, dense water formation and outflow on the northeast Chukchi Shelf. *J. Geophys. Res.*, **103**, 7647–7661..

Willmott, A. J., and M. A. Morales Maqueda, 1997: A model for the influence of wind and oceanic currents on the size of a steady-state latent heat coastal polynya. *J. Phys. Oceanogr.*, **27**, 2256–2275.. [Find this article online](#)

APPENDIX

6. Ocean Response during Polynya Opening

As the Pease model polynya opens, the amount of time that each offshore location is exposed to the surface buoyancy flux varies. If y is the offshore coordinate measured from the coast, then location $y < b$ has been exposed for a time interval

$$\Delta t = t + \frac{\kappa}{B_0} \ln(1 - y/b_{\max}), \quad (\text{A1})$$

where t is the present time and (12) has been used. The maximum of (A1) is the negative of the time at which the polynya edge reached y . Note that $\Delta t = t$ at the coast $y = 0$, and $\Delta t = 0$ at the polynya edge $y = b$. Eddies are not a factor during the initial polynya opening, so the surface buoyancy flux increases the water density by

$$\Delta\rho = \frac{\rho_0 B_0}{gH} \left[t + \frac{\kappa}{B_0} \ln(1 - y/b_{\max}) \right] \quad (\text{A2})$$

according to (3). The maximum geostrophic velocity that develops from this density anomaly can be estimated from the thermal wind, assuming that the velocity is vertically antisymmetric:

$$\mathbf{v}_{\max} = -\frac{gH}{2\rho_0 f} \frac{\partial \Delta\rho}{\partial y} = \frac{\kappa}{2fb_{\max}} \left(\frac{1}{1 - y/b_{\max}} \right). \quad (\text{A3})$$

The density anomaly is largest at the coast, but the density gradient and, therefore, the velocity are largest at the polynya edge. Interestingly, the velocity is independent of time, so the geostrophic velocity does not change at each location once the polynya edge has passed. This occurs because the density gradient is set as the polynya edge passes, and continued exposure to the surface buoyancy flux simply increases the density by the same amount everywhere, leaving the density gradient unchanged. The polynya opens so rapidly that the velocity produced is small except near the polynya edge and is unimportant to the ocean response on longer time scales. For example, with $b_{\max} = 15$ km, $\kappa = 0.0165 \text{ m}^2 \text{ s}^{-2}$, and $f = 1.3 \times 10^{-4} \text{ s}^{-1}$, the velocity from (A3) only reaches 0.05 m s^{-1} at $y = 13.7$ km, very close to the polynya edge.

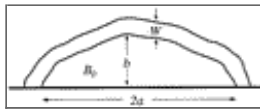
Tables

Table 1. Polynya area A and perimeter P for various idealized shapes. The infinite strip alongshore length $2a$ is included only to allow A/P to be computed. Here E is the complete elliptic integral of the second kind.

Shape	A	P	A/P
Infinite strip	$2ab$	$2a$	b
Rectangle	$2ab$	$2a + 2b$	$-b$ for $b \ll a$
Half-circle	$\pi b^2/2$	πb	$b/2$
Half-ellipse	$\pi ab/2$	$2aE(1 - b^2/a^2)$	$\pi b/4E(1 - b^2/a^2)$

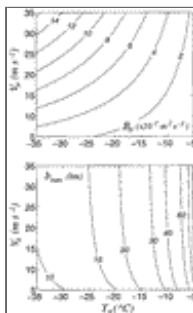
[Click on thumbnail for full-sized image.](#)

Figures



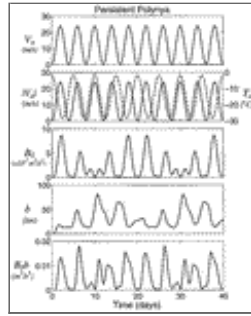
[Click on thumbnail for full-sized image.](#)

Fig. 1. Generalized coastal polynya geometry with length $2a$ along a straight coast and extending offshore a distance b at its widest point. Constant surface buoyancy flux B_0 is applied within the inner region, decreasing to zero across the forcing decay region of width W .



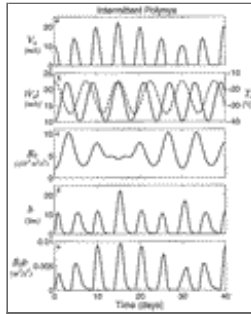
[Click on thumbnail for full-sized image.](#)

Fig. 2. Surface buoyancy flux B_0 (upper) and maximum width b_{\max} (lower) from the Pease polynya model with constant forcing, computed using (11) and (13) with various air temperatures T_a and offshore wind speeds V_a .



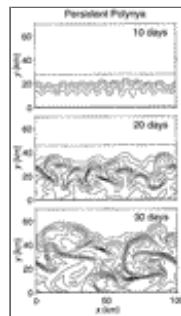
Click on thumbnail for full-sized image.

Fig. 3. Persistent polynya response to periodic air temperature and wind speed given by (15) and (16), respectively, with $T_0 = -15^\circ\text{C}$, $T_1 = 13.2^\circ\text{C}$, $\omega_T = 2\pi/5$ days, $V_0 = 12 \text{ m s}^{-1}$, $V_1 = -12 \text{ m s}^{-1}$, $\omega_m = 2\pi/4$ days, and $\omega_o = 0$. The dashed curve in (b) is T_a .



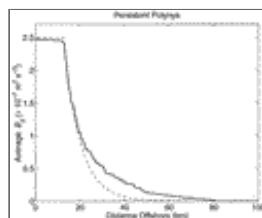
Click on thumbnail for full-sized image.

Fig. 4. Intermittent polynya response to periodic air temperature and wind speed given by (15) and (16), respectively, with $T_0 = -25^\circ\text{C}$, $T_1 = 10^\circ\text{C}$, $\omega_T = 2\pi/7.5$ days, $V_0 = 16 \text{ m s}^{-1}$, $V_1 = -6 \text{ m s}^{-1}$, $\omega_m = 2\pi/6$ days, and $\omega_o = 2\pi/5$ days. The dashed curve in (b) is T_a .



Click on thumbnail for full-sized image.

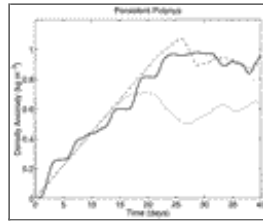
Fig. 5. Plan views of density anomaly at the ocean bottom for the persistent polynya forcing in Fig. 3 after 10, 20, and 30 days. Contours are 0.075 to 1.2 by 0.075 kg m^{-3} with the minimum contour farthest offshore. The full model domain extends 100 km offshore.



Click on thumbnail for full-sized image.

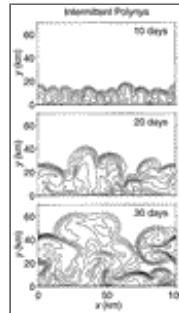
Fig. 6. The solid curve is the 40-day average surface buoyancy flux as a function of distance offshore for the persistent polynya forcing in Fig. 3. The dashed curve is an approximation to the average; $B_0 = 2.5 \times 10^{-7} \text{ m}^2 \text{ s}^{-3}$ out to 12.5 km

offshore, adjoined to an exponential decay with an e -folding scale of 7.5 km.



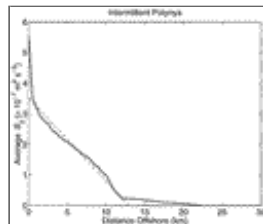
[Click on thumbnail for full-sized image.](#)

Fig. 7. The solid curve is the density anomaly near the coast (averaged along the coast and within 4 km offshore) versus time for the persistent polynya forcing shown in [Fig. 3](#). The dashed curve is the response to the approximate average forcing shown by the dashed curve in [Fig. 6](#). The dotted curve is the response to steady forcing with no forcing decay region; $B_0 = 2.5 \times 10^{-7} \text{ m}^2 \text{ s}^{-3}$ out to 12.5 km offshore and zero beyond.



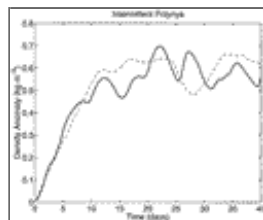
[Click on thumbnail for full-sized image.](#)

Fig. 8. Plan views of density anomaly at the ocean bottom for the intermittent polynya forcing in [Fig. 4](#) after 10, 20, and 30 days. Contours are 0.075 to 0.75 by 0.075 kg m^{-3} with the minimum contour farthest offshore. The full model domain extends 100 km offshore.



[Click on thumbnail for full-sized image.](#)

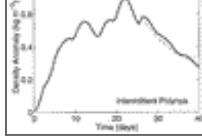
Fig. 9. The solid curve is the 40-day average surface buoyancy flux as a function of distance offshore for the intermittent polynya forcing shown in [Fig. 4](#). The dashed curve is an approximation to the average; $B_0 = 3.5 \times 10^{-7} \text{ m}^2 \text{ s}^{-3}$ at the coast and decreasing linearly to zero 13 km offshore.



[Click on thumbnail for full-sized image.](#)

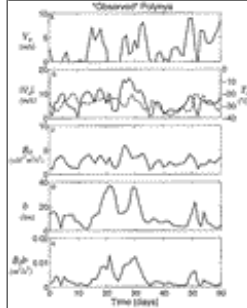
Fig. 10. The solid curve is the density anomaly near the coast (averaged along the coast and within 4 km offshore) versus time for the intermittent polynya forcing shown in [Fig. 4](#). The dashed curve is the response to the approximate average forcing shown by the dashed curve in [Fig. 9](#).





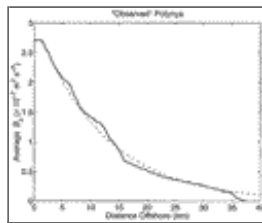
Click on thumbnail for full-sized image.

Fig. 11. Density anomaly near the coast, as in [Figs. 7](#) and [10](#), except that the forcing ceases at day 30 for the persistent polynya in (a) and at day 26.5 for the intermittent polynya in (b). The dashed curves are given by [\(7\)](#); $\rho_e = 0.9 \text{ kg m}^{-3}$, $t_e = 20$ days, and $t_c = 30$ days in (a), $\rho_e = 0.6 \text{ kg m}^{-3}$, $t_e = 13$ days, and $t_c = 26.5$ days in (b).



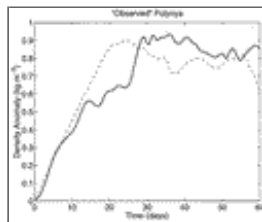
Click on thumbnail for full-sized image.

Fig. 12. “Observed” daily values of the polynya forcing parameters based on data from [Weingartner et al. \(1998\)](#). Day 0 corresponds to 20 December 1991. See text for more details. The dashed curve in (b) is T_a .



Click on thumbnail for full-sized image.

Fig. 13. The solid curve is the 60-day average surface buoyancy flux as a function of distance offshore for the “observed” forcing shown in [Fig. 12](#). The dashed curve is an approximation to the average; $B_0 = 2.7 \times 10^{-7} \text{ m}^2 \text{ s}^{-3}$ out to 1.5 km offshore, adjoined to an exponential decay with an e -folding scale of 12 km.



Click on thumbnail for full-sized image.

Fig. 14. The solid curve is the density anomaly near the coast (averaged along the coast and within 4 km offshore) versus time for the “observed” forcing shown in [Fig. 12](#). The dashed curve is the response to the approximate average forcing shown by the dashed curve in [Fig. 13](#).

¹ The equilibrium quantities [\(4\)](#) and [\(5\)](#) were derived assuming a linear forcing decay region with total width W . However, an exponential forcing decay region produces the same relationships but with W being the e -folding scale.

* Woods Hole Oceanographic Institution Contribution Number 9714.

Corresponding author address: Dr. David C. Chapman, Dept. of Physical Oceanography, Woods Hole Oceanographic Institution, Woods Hole, MA 02543.

E-mail: dchapman@whoi.edu



© 2008 American Meteorological Society [Privacy Policy and Disclaimer](#)

Headquarters: 45 Beacon Street Boston, MA 02108-3693

DC Office: 1120 G Street, NW, Suite 800 Washington DC, 20005-3826

amsinfo@ametsoc.org Phone: 617-227-2425 Fax: 617-742-8718

[Allen Press, Inc.](#) assists in the online publication of *AMS* journals.